ELLIPTICAL PIN FINS AS AN ALTERNATIVE TO CIRCULAR PIN FINS FOR GAS TURBINE BLADE COOLING APPLICATIONS

Part 1 : Endwall Heat Transfer and Total Pressure Loss Characteristics

Oğuz Uzol [*], **Cengiz Camci**
Turbomachinery Heat Transfer Laboratory
Department of Aerospace Engineering
Pennsylvania State University
University Park, PA 16802

ABSTRACT

Detailed experimental investigation of the wall heat transfer enhancement and total pressure loss characteristics for two alternative elliptical pin fin arrays is conducted and the results are compared to the conventional circular pin fin arrays. Two different elliptical pin fin geometries with different major axis lengths are tested, both having a minor axis length equal to the circular fin diameter and positioned at zero degrees angle of attack to the free stream flow. The major axis lengths for the two elliptical fins are 1.67 and 2.5 times the circular fin diameter, respectively. The pin fin arrays with H/D = 1.5 are positioned in a staggered 2 row configuration with 3 fins in the first row and 2 fins in the second row with S/D = X/D = 2. Endwall heat transfer and total pressure loss measurements are performed two diameter downstream of the pin fin arrays (X/D = 2) in a rectangular cross-section tunnel with an aspect ratio of 4.8 and for varying Reynolds numbers between 10000 and 47000 based on the inlet velocity and the fin diameter. Liquid Crystal Thermography is used for the measurement of convective heat transfer coefficient distributions on the endwall inside the wake. The results show that the wall heat transfer enhancement capability of the circular pin fin array is about 25-30% higher than the elliptical pin fin arrays in average. However in terms of total pressure loss, the circular pin fin arrays generate 100-200% more pressure loss than the elliptical pin fin arrays. This makes the elliptical fin arrays very promising cooling devices as an alternative to conventional circular pin fin arrays used in gas turbine blade cooling applications.

[1]Currently at the Department of Mechanical Engineering, Johns Hopkins University, Baltimore MD 21218

NOMENCLATURE

A	Surface area
D	Circular Fin diameter, Elliptical Fin minor axis length
f	Friction coefficient (Total pressure loss coefficient)
h	Convective heat transfer coefficient
H	Pin fin height
HSI	Hue Saturation Intensity
k	Thermal conductivity
Nu_D	Nusselt number based on D
P_t	Total pressure
Pr	Prandtl number
q''	Heat flux on the heater strip
RGB	Red Green Blue
R	Resistance
Re_D	Reynolds number based on D
S	Pin fin array spanwise spacing
SEF	Standard Elliptical Fin
t	Thickness
T	Temperature
Tu	Turbulence intensity
u	Velocity
V	Voltage
X	Pin fin array streamwise spacing

Subscripts :

∞	Free stream
2	Ambient side of the endwall
av	Average
cond.	Conduction loss
exit	Inside the wake
hs	Heater strip

in	Inlet
rad.	Radiation loss
Total Gen.	Total Generated
tunnel	Baseline empty tunnel value
wall	Endwall surface

Greek Symbols:

ε_∞	Tunnel wall surface emissivity
ε_f	Specific friction loss
ε_{wall}	Heater strip surface emissivity
ρ	Density
σ	Stefan-Boltzmann constant

INTRODUCTION

In order to obtain increased thrust levels and decreased fuel consumption rates for gas turbine engines, higher levels of turbine inlet temperatures are necessary. This need for higher temperatures results in a demand for effective internal and external cooling techniques for the high pressure turbine blades. In-line and staggered arrays of short cylindrical pin fins with circular cross-sections are one of the most common types of cooling devices used in turbine blades. These pin fin arrays enhance the heat transfer levels both by increasing the pin fin wetted surface area and the passage thermal transport downstream of the pin fin. However it is by no means clear that the circular cylinder is the most efficient geometry in terms of heat transfer enhancement and pressure loss minimization.

The past pin fin research is mostly based on the determination of heat transfer and pressure loss characteristics of different array configurations with circular pin fins. Nevertheless, there has also been some effort in investigating different pin fin shapes and concepts. Steuber and Metzger [1] investigated partial length circular pin fins as an alternate to full circular pin fins. Their results showed that the partial length pin fins did not outperform the full length fins in terms of heat transfer but when the heat transfer and pressure loss are both considered, some of their partial length pin fin arrays were superior. Arora and Abdel-Messeh [2] also investigated the partial length circular pin fin concept and found that both the array averaged heat transfer and friction factor decreases with increasing gap distance. Pin fins with oblong cross-sections are investigated by Metzger et al. [3] for various pin orientations with respect to the main flow. Their results indicate that the use of elongated pin fins (oblong shape) increases endwall heat transfer but also causes higher levels of aerodynamic penalty than the circular pin fins when the main flow direction deviates from the direction of the major axis of the oblong pin fin. When the main flow approaches with zero incidence, the pressure loss levels become lower than that of circular pin fins. Wang and Ji [4] experimentally investigated the heat transfer and pressure loss characteristics of tapered pin fin configurations and compared their results with full cross pin fins and shorter round pin fins. This comparison showed that the tapered pin fins had the smallest specific friction loss (f/Nu). A numerical investigation of the flow through diamond shaped pin fin arrays is performed by Grannis and Sparrow [5] using a finite element based solution method. They compared their predictions of per row pressure drop with the experimental data and achieved satisfactory agreement. A flow visualization study along with heat transfer measurements for in-line circular and square pin fins is conducted by Minakami et al. [6]. Test results showed that the circular pin fin array had higher heat transfer levels and this was explained by wider flow mixing area created in circular pin fin arrays than in case of the square pin fins. In terms of pressure loss the square and circular pin fins had similar overall performances. Stepped diameter circular fin arrays have been investigated by Goldstein et al. [7] in a Reynolds number range 3000 to 18000 based on the approach velocity and fin diameter and for a 10 row staggered array. It is found that the stepped diameter circular fins have a smaller pressure loss and higher heat transfer rates compared to the uniform diameter circular pin fin arrays. Chyu et al. [8] investigated the heat transfer and pressure loss characteristics of cubic and diamond shaped pin fin arrays for both in-line and staggered configurations. The arrays they have used had geometric parameters H/D = 1, S/D = X/D = 2.5. They have found that the cubic pin fin arrays produced the highest heat transfer rates (contrary to Minakami et al. [6]) than the diamond and circular fins and the diamond pin fin array induced the greatest pressure loss. As a result of this study the cubical pin fin arrays were proposed as viable alternatives to circular pin fins for internal cooling of the blade trailing edge. Li et al. [9] investigated elliptical pin fin arrays for Reynolds numbers between 900 and 9000. The major and minor axis of the elliptical fins is chosen such that their circumference is equal to the circumference of a corresponding circular pin fin. This approach resulted in smaller effective frontal areas for the elliptical fins which naturally led to lower total pressure loss levels than the circular pin fins. However this kind of approach was necessary since the heat transfer levels on the pin itself were going to be measured and compared with that of a circular pin fin. They have found that the heat transfer of a channel with elliptic pin fins is somewhat higher than that with circular pin fins. Chen et al. [10] conducted similar experiments with drop-shaped pin fins, again using the equal circumference diameter concept. They have also found much less pressure loss levels for drop-shaped pin fins, but similar to Li et al. [9] this was mainly due to the smaller frontal area of the drop-shaped fins in order to achieve the same surface area with the corresponding circular fins. The heat transfer levels of drop-shaped pin fin arrays were found higher than the levels for circular pin fin arrays as a result of this study.

In this study two different types of elliptical pin fins are investigated in a staggered array configuration as an alternative to the conventional circular pin fins used in gas turbine blade cooling and the results are compared. The first type has a standard elliptical cross-section similar to the fins used by Li et al. [9],

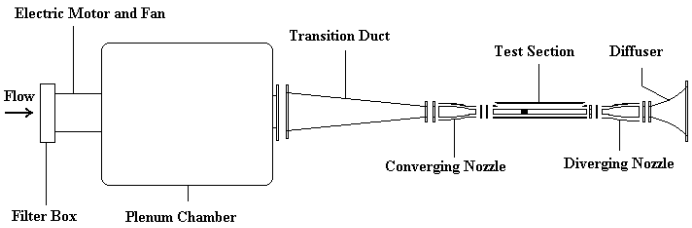

Figure 1. Low Speed Heat Transfer Research Facility

however with a different major to minor axis ratio. The second type of elliptical fins are derived from NACA four digit symmetrical airfoil series and this is the first time they are being introduced and investigated. The minor axis length for both types of elliptical fins are kept equal to the diameter of the circular fins in order to obtain the same effective frontal area. The minor axis length of the elliptical fins used by Li et al. [9] was smaller than the corresponding circular fin diameter in order to obtain the same surface area on the fins. Detailed endwall heat transfer and total pressure loss measurements are conducted for 2 row staggered array configurations. The objective was to obtain and compare line distributions of the convective heat transfer coefficients on the endwall and total pressure loss inside the wake for elliptical and circular pin fin arrays.

EXPERIMENTAL SETUP AND PROCEDURE

Facility

The experiments are conducted at the "Low Speed Heat Transfer Research Facility" at the Turbomachinery Heat Transfer Laboratory of the Pennsylvania State University. This is an open loop wind tunnel which consists of an axial air blower, a diffuser with multiple screens, a plenum chamber, a high area ratio circular nozzle, a circular to rectangular transition duct, a converging nozzle, the test section, a diverging nozzle and a diffuser. The schematic of the facility is shown in Figure 1.

An axial flow fan is used to draw the ambient air into the facility. A 66cm x 66cm x 38.7 cm filter box encloses the inlet of the axial fan. A 7.5 kW electric motor drives the 45.7 cm tip diameter fan which has a potential to provide a pressure differential of 15 cm of water over a range of flow rates. The speed of the electric motor is controlled by using an adjustable frequency AC drive. After the fan the air blows through a series of screens and enters a 1.73 m^3 plenum chamber. Downstream of the plenum the air accelerates through a circular nozzle of area ratio 8.65 then transitions to a 36.67 cm x 15.24 cm rectangular cross-section by a 137 cm long duct. The cross-section is further reduced to 36.67 cm x 7.62 cm by a converging nozzle which is 50.8 cm long and also has a rectangular cross-section. After the converging nozzle there is the test section which is a 127 cm long

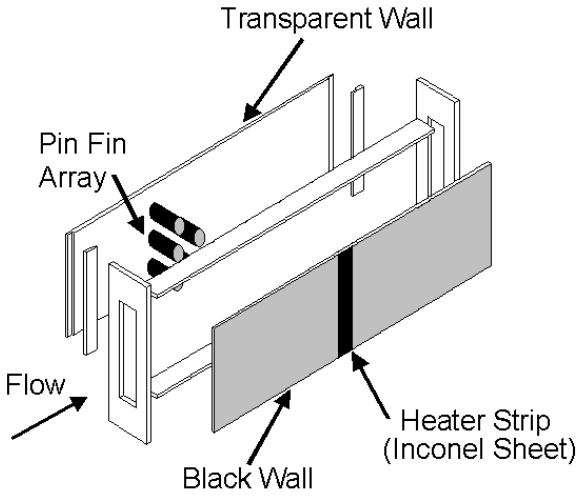

Figure 2. Test Section

straight rectangular duct made out of 1.27 cm thick clear acrylic. It has a 36.67 cm x 7.62 cm cross-section and is illustrated in Figure 2.

The pin fin arrays are placed approximately 4D downstream from the entrance of the test section in which the flow properties are not fully developed but developing. The duct continues up to 10D downstream of the arrays. Here D is the diameter of a single circular fin. The height to diameter ratio (H/D) of the pin fins is 1.5 which is a typical value for turbine blade cooling applications. The pin fins commonly used in turbine cooling have pin H/D ratios between 1/2 and 4 due to blade size and manufacturing constraints(Armstrong and Winstanley [12]). The pin fin arrays are placed inside the test section in a staggered array configuration consisting of 2 rows of fins, with 3 fins in the first row and 2 fins in the second row as illustrated in Figure 4. The transverse and streamwise distance between each fin is taken equal to the diameter of the circular fin such that S/D = X/D = 2. Using only two rows of pin fins may not be enough to establish a fully developed pattern inside the test section, however, it was useful for determining the relative endwall heat transfer enhancement and total pressure loss minimization performances of arrays with different fin shapes.

Pin Fin Geometries

One circular and two different elliptical pin fin shapes are tested and the results are compared. The elliptical pin fin shapes are explained as follows :

The Standard Elliptical Fin (SEF) This pin fin has a standard elliptical cross-section with the minor axis length being equal to the circular fin diameter and the major axis length is 1.67 times the minor axis length. The geometry and the relative

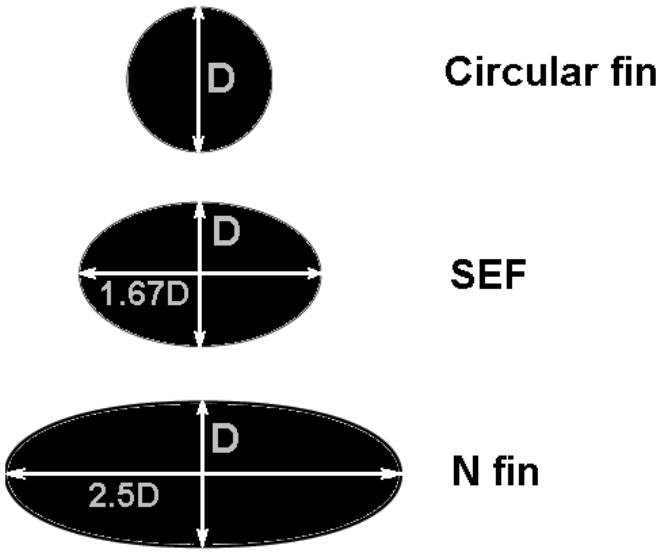

Figure 3. Relative Dimensions of the Circular Fin, SEF and the N fin

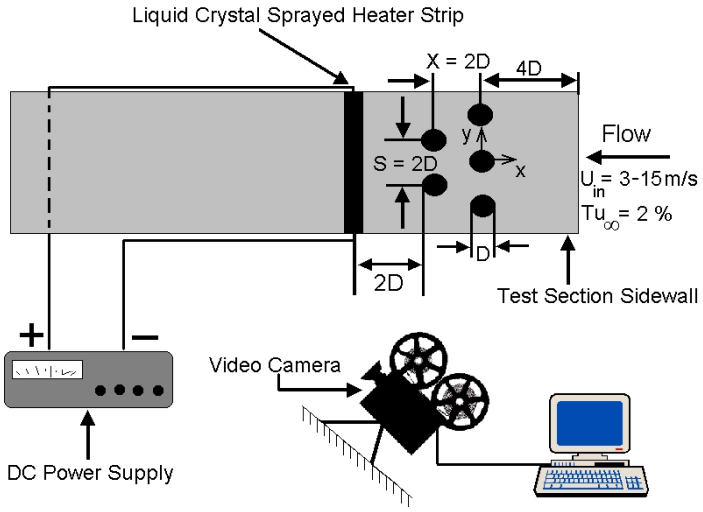

Figure 4. Experimental Setup for Endwall Heat Transfer Measurements

dimensions of the SEF is given in Figure 3. The surface area of SEF is calculated to be 1.35 times the surface area of the circular fin, but the effective frontal areas are the same for both fins since the minor axis length is equal to the circular fin diameter. This is important in order to be able to make comparisons of the aerodynamic penalty levels for those geometries. Increased surface area will result in increased heat transfer levels on the pin itself but measurements on the pin is beyond the scope of this study. Only the endwall heat transfer enhancement inside the wakes is considered.

The N Fin This fin shape is derived from the NACA four-digit symmetrical airfoil series. The thickness distribution for the four-digit series of airfoils is given in Abbott and Von Doenhoff [13] as

$$y = \frac{t}{0.2}(0.29690\sqrt{x} - 0.12600x \\ -0.3516x^2 + 0.2843x^3 - 0.1015x^4) \quad (1)$$

where t is the maximum thickness as a fraction of the chord length. This distribution gives the maximum thickness at 30% chord location. In order to obtain the N fin shape the NACA 0024 airfoil is taken as a basis, which has 24% maximum thickness, and only the airfoil geometry upto the maximum thickness location is used to construct the forward half of the fin. The backward part is constructed by taking the mirror image of the forward half. Figure 3 shows the N fin geometry and the relative dimensions of the N fin with respect to the circular pin fin. The minor axis length is equal to the diameter of the circular fin and the major axis length is 2.5 times the minor axis length. The surface area of the N fin is calculated to be 1.85 times larger than the surface area of the circular fin. The effective frontal areas are the same for both fins.

Endwall Heat Transfer Measurement Procedure

Measurements for convective heat transfer coefficients on the endwall downstream of the pin fin arrays are performed using liquid crystal thermography. For this purpose a rectangular heater strip, 2.54 cm wide (0.5D) and 41.9 cm high (8.2D), is placed 2D downstream of the model and attached on the tunnel sidewall. Although the width of the heater strip is small compared to the pin fin diameter and tunnel dimensions, it was sufficient for obtaining line distributions of the convective heat transfer coefficient along the centerline of the heater strip. The heater strip height allowed a 1.27 cm excess on either end of the strip for bus bar connections to the DC power supply. Figure 4 shows the experimental setup for the convective heat transfer coefficient measurements. The heater strip, made out of Inconel 600 foil, is attached to the sidewall using double sided tape. The Inconel 600 foil is a low resistivity steel foil (75% Ni, 15% Cr, 10% Fe) which has a low temperature coefficient resistivity that restrained a change in the resistance of the foil within the temperature range used in the experiments. The strip surface is then painted black in order to obtain the best color contrast for the liquid crystals. A thin coat of liquid crystals with an event temperature of approximately 45^o and a band width of 1^o is sprayed onto the heater strips after the black paint is applied. After the heater strip is prepared and the pin fin array is placed inside the test section, the tunnel is started and a DC voltage is applied across the heater strip. The applied DC voltage results in an increase in the surface temperatures on the heater strip which in

turn results in the appearance of color bands on the surface due to the thermochromic properties of the liquid crystal material. The DC voltage is started from zero and slowly increased until the color bands started to appear. At this point steady state conditions are allowed to be reached and then a 352x240 pixel image of the heater strip is captured in bitmap format through a video camera and a computer. The color information on the heater strip is directly related to the surface temperature. After the image is recorded the power to the heater strip is then increased causing a shift in the position of the color bands. This process is repeated until the color bands have covered the entire heater strip surface. The illumination during this procedure is supplied by two 150 Watts incandescent light bulbs in reflectors positioned on either side of the test section. Direct radiative heating of the liquid crystal coated surface is minimized by only illuminating the lights when data were being taken.

Image Processing Technique After the recording phase of the images is finished, the images are analyzed one by one to obtain the hue, saturation and intensity information on the heater strip. The hue attribute is used to determine the surface temperature at a given pixel location on the image and intensity is used as a filtering device. Intensity values lower than 50 usually causes the hue values to become unstable and the pixel can not be used to obtain the accurate temperature (Camci et al. [14]). Also if the intensity value of a pixel exceeds 200, the hue value becomes less accurate due to the saturation of the sensor in the video camera. The image processing procedure is as follows :

1. The RGB information at each pixel on the image is extracted from the bitmap file.

2. The extracted RGB information is converted to HSI values for the the pixel column corresponding to the heater strip on the image. The RGB to HSI conversion is performed using standard conversion formulas (Niblack [15] and Russ [16]).

3. For each pixel row on the heater strip, hue values of pixels around the centerline of the heater strip are determined. Then a filtering process using the intensity values is performed for these pixels such that any pixels with intensity values less than 50 and higher than 200 are rejected. Also if the hue value for a pixel is outside the calibration range, that pixel is not considered. Using this filtering procedure, the valid pixels around the centerline are determined and the endwall temperature values for the valid pixels are calculated using the calibration curve. These temperature values aruond the centerline are then used for determining the average temperature on the centerline of the heater strip for each power setting. The minimum number of valid pixels used in this averaging process is also controlled such that if this number is below a certain value, that pixel row is skipped.

4. The convective heat transfer coefficient at the centerline of the heater strip at each pixel row is then calculated from Newton's Law of Cooling.

$$h = \frac{q''_{TotalGen.} - q''_{cond.} - q''_{rad.}}{T_{wall} - T_{\infty}} \tag{2}$$

The total generated heat flux on the rectangular heater strip is calculated from Joulean heating,

$$q''_{TotalGen.} = \frac{V_{hs}^2}{R_{hs} A_{hs}} \tag{3}$$

where V_{hs} is the voltage across the heater strip, R_{hs} is the resistance of the heater strip and A_{hs} is the area of the heater strip. It must be noticed that equation 3 is valid only for rectangular heater geometries with any aspect ratio. A more detailed technique to calculate the total generated heat for arbitrarily shaped boundaries is explained in detail in Wiedner and Camci [17].

The conduction heat loss term is obtained using,

$$q''_{cond.} = k_{wall} \frac{T_{wall} - T_2}{t_{wall}} \tag{4}$$

Here T_{wall} is the surface temperature on the heater strip, T_2 is the temperature on the ambient side of the wall and t_{wall} is the wall thickness. The temperature on the ambient side of the wall (T_2) is also measured using a K-type cement-on thermocouple attached on the wall surface at the ambient side.

The radiation heat loss term is estimated by using a black body assumption. Hence,

$$q''_{rad.} = \sigma \varepsilon_{wall} T_{wall}^4 - \sigma \varepsilon_{\infty} T_{\infty}^4 \tag{5}$$

where σ is the Stefan-Boltzmann constant, ε_{wall} and ε_{∞} are the heater strip and tunnel wall surface emissivities, respectively. The freestream static temperature, T_{∞}, is taken equal to the total temperature at the test section inlet which was measured at that location. This is a valid assumption since the Mach numbers in the test section are very low for the current experiments.

Measured convective heat transfer coefficient values are then used to calculate the Nusselt numbers using,

$$Nu_D = \frac{hD}{k_{air}} \tag{6}$$

where D is the diameter of the circular fin and k_{air} is determined using the inlet static temperature.

Thermal Boundary Layer on the Heater Strip Due to the nature of the measurement technique, there exists a developing thermal boundary layer along the width of the heater strip. The character of this thermal boundary layer will be similar for each pixel row on the heater strip such that the convective heat transfer coefficients will start from a maximum and will decrease as the thermal boundary layer develops. However the levels of heat transfer enhancement will be different along the length of the heater strip depending on the relative location of the pixel row with respect to the wake of the pin fin array. The main objective of the current experiments is to capture these differences in the levels of heat transfer enhancement for pin fin arrays with different fin shapes which have different wake characteristics.

Liquid Crystal Calibration The sprayed liquid crystals on the heater strip are calibrated before starting the wall heat transfer measurements. For this purpose a K-type cement-on thermocouple is attached on the surface of the heater strip before the strip is painted black and coated with liquid crystals. Then the test section wall instrumented with the heater strip is installed on the tunnel. The illumination lights and the video camera are positioned to record the color response on the heater strip with the thermocouple, along with a voltmeter readout of the thermocouple voltage in the same field of view. The positions of the lights are remained constant both for the calibration and the actual heat transfer experiments. A DC voltage is applied across the heater strip until the color bands appear and a slow color transient is achieved over the thermocouple while the heater strip is cooling. Images of the heater strip is captured during this cooling process and the pixel overlaying the thermocouple sensor location is analyzed for hue information.

The instantaneous thermocouple voltage is converted to a temperature value through the calibration slope of the thermocouple. This process is repeated and a hue vs. temperature calibration plot is constructed as shown in Figure 5.

It can be seen from the calibration plot that a useful linear range exists between hue values 30 and 150, for this specific liquid crystal mixture. A line is drawn through this range and the slope is used to obtain the temperature information on the heater strip using,

$$Hue = 118.81T - 5356.93 \tag{7}$$

The uncertainty in the measurement of the temperature value from the hue value in the linear range can be estimated as $\pm 0.20^oC$. However including the uncertainty in the thermocouple measurement, the overall uncertainty is $\pm 0.30^oC$.

The Hue vs. Intensity variation is a useful tool to determine whether the intensity boundaries are exceeded. It is explained in Camci et al. [14] that if the intensity drops below 50,the color image sensors do not provide accurate hue values. Also for

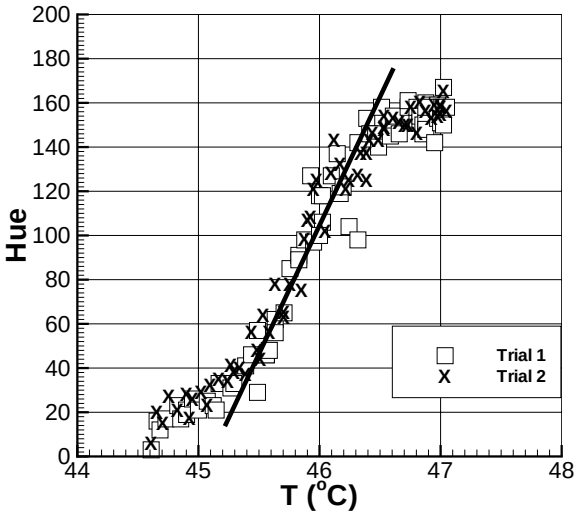

Figure 5. Hue vs. Temperature Calibration Curve

intensity values higher than 200, the accuracy of the hue value suffers due to the saturation of the CCD sensor. The intensity values for the current experiments are mostly around 100 in the useful hue range.

Total Pressure Loss Measurement Procedure

Total pressure levels inside the wakes of the pin fin arrays are determined by traversing a kiel probe with 3.175 mm shield diameter across the test section again 2D downstream of the pin fin arrays. Measured total pressure data are used to calculate relative pressure loss created with respect to the inlet conditions. The total pressure loss coefficient (or friction coefficient) can be defined as,

$$f = \frac{P_{t_{in}} - P_{t_{exit}}}{\frac{1}{2}\rho u_\infty^2} \tag{8}$$

The inlet static pressure, total pressure and inlet velocity are measured 4D upstream of the pin fin arrays using a pitot-static probe.

RESULTS AND DISCUSSION

Endwall Heat Transfer Measurements

The wall heat transfer measurements for the circular, SEF and N fin arrays are conducted for six different Reynolds numbers varying between 10000 - 47000 which are calculated using the test section inlet velocity and the fin diameter (or SEF minor axis length). The test section inlet velocity changes between

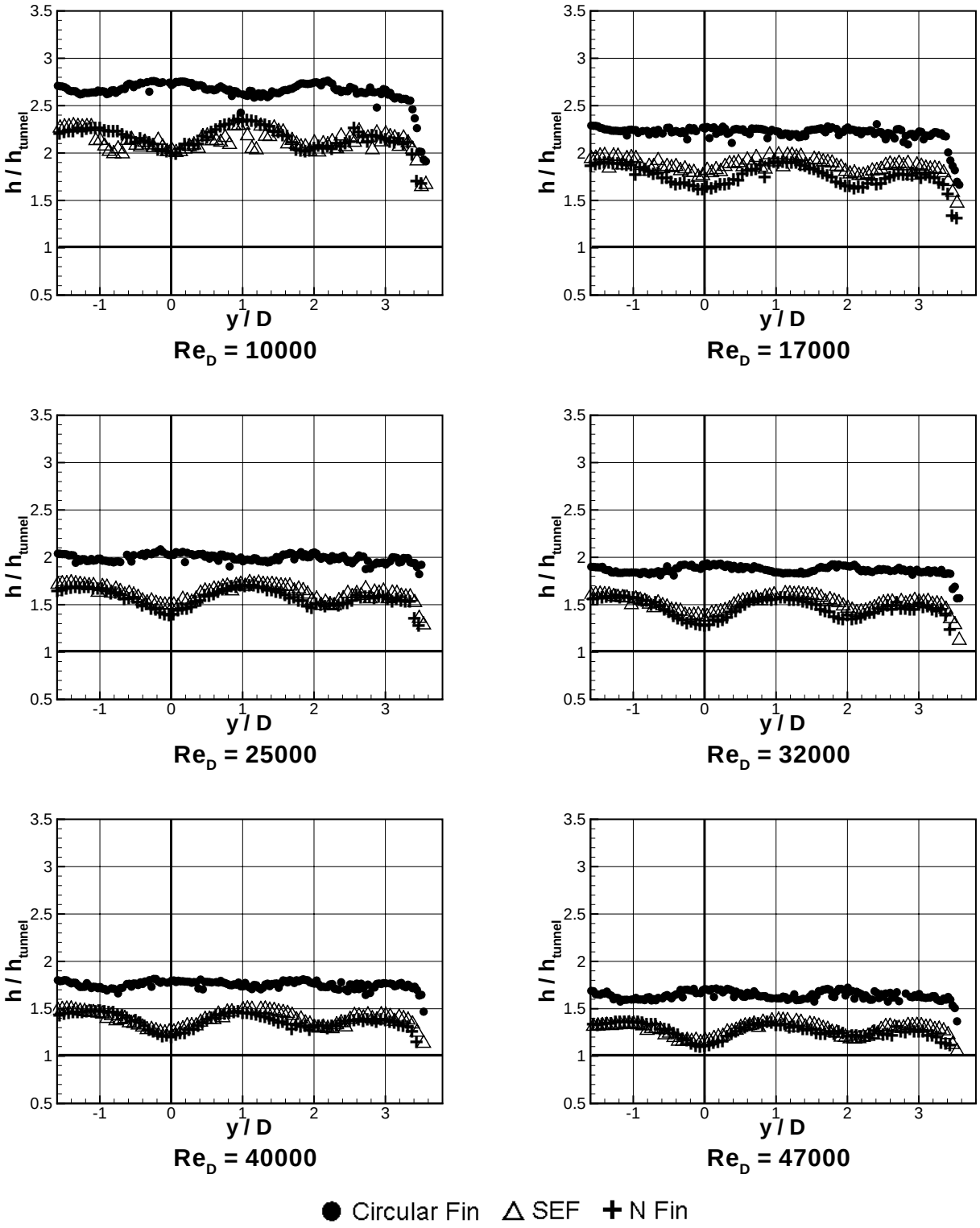

Figure 6. Convective Heat Transfer Coefficient Distribution for Circular, SEF and N fin Arrays-2D Downstream (Relative Values over the Baseline Empty Tunnel Values) (X/D = 2)

3 m/s to 15 m/s in this Reynolds number range. The inlet turbulence intensity level is 2%. The distributions of the wall heat transfer enhancement levels over the baseline tunnel values inside the wakes of the arrays, obtained from the measurements are illustrated in Figure 6. In case of the circular fin array, the heat transfer enhancement levels are higher than the levels for the SEF and N fin arrays, in the Reynolds number range. The levels for the SEF and N fin arrays are very close to each other which indicates that the wake characteristics of these two devices should be similar. Local enhancements of the endwall heat transfer inside the wakes of the SEF and N fin arrays is also visible in the form of two peaks in the line distributions. However for circular fin arrays these local enhancements are not observed. This indicates that the flow is much better mixed in the wakes of circular fin arrays. The effect of the individual wake zones can not be observed whereas they are visible for elliptical pin fins.

Figure 7 shows the average Nusselt number variation with Reynolds Number for the fin arrays in a log-log scale arrangement. The uncertainty in the Nusselt numbers are calculated to be $\pm 4\%$ using the root-sum-square method described in Moffat [18]. A linear variation in log-log coordinates with Reynolds number for all arrays can be seen from this figure. The equations for the best fit lines are

Circular Fin,

$$Nu_D = 0.208 Re_D^{0.696} Pr^{0.3} \tag{9}$$

SEF,

$$Nu_D = 0.203 Re_D^{0.675} Pr^{0.3} \tag{10}$$

N Fin,

$$Nu_D = 0.219 Re_D^{0.665} Pr^{0.3} \tag{11}$$

The Nusselt number variation for the empty tunnel measurements are also presented in Figure 7. The Reynolds number values for the empty tunnel measurements are calculated using the test section inlet velocity and the pin fin diameter, similar to the pin fin array measurements. The correlation for the Nusselt number variation for a flat plate with a turbulent boundary layer is also plotted as a reference (Incropera and De Witt [19]). It can be observed that the empty tunnel measurements show a similar trend to the flat plate characteristics. The equations for the empty tunnel and the flat plate are,

Empty tunnel,

$$Nu_D = 0.0401 Re_D^{0.781} Pr^{0.3} \tag{12}$$

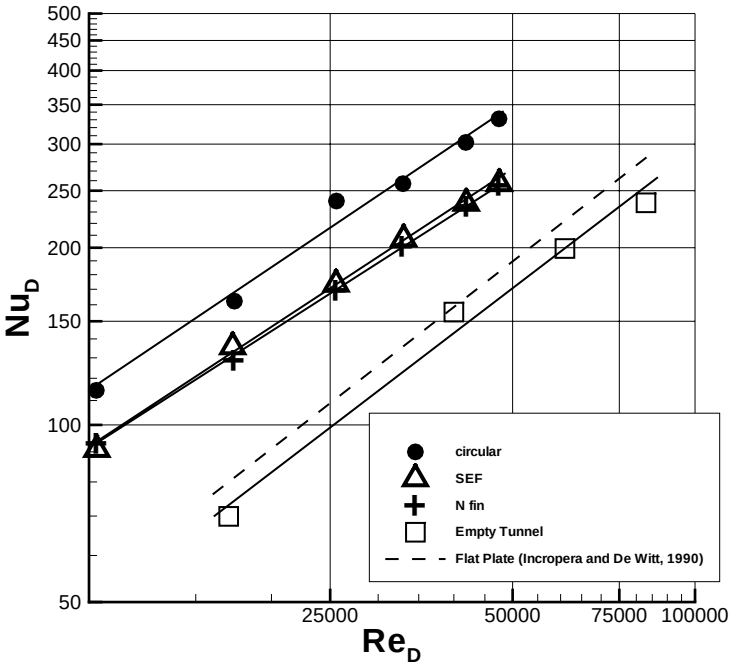

Figure 7. Nusselt Number vs. Reynolds Number for Circular, SEF and N Fin Arrays

Flat plate (Incropera and De Witt [19]),

$$Nu_D = 0.037 Re_D^{0.8} Pr^{0.3} \tag{13}$$

The levels for the circular fin are always higher than the levels for the SEF and N fin arrays. For the lowest Reynolds number, the average Nusselt number for the circular fin array is 26% and 23% higher than the average Nusselt numbers for the SEF and N fins, respectively. Similarly for the highest Reynolds number the heat transfer level for the circular fin array is 28.8% and 29.5% higher than the respective values of the SEF and the N fin arrays. Therefore in terms of heat transfer enhancement inside the wake, the circular fin array performs better than the others. However the pressure loss characteristics of these arrays should also be considered in order to be able to compare the performance levels of these pin fin arrays.

Total Pressure Loss Measurements

The experiments are conducted in the same Reynolds number range as in the endwall heat transfer measurements, i.e. 10000 - 47000. Measured total pressure values inside the wake are converted to friction coefficient values (Equation 8) which is an indication of the local pressure loss created with respect to the inlet values.

Figure 8 shows the measured friction coefficient distributions inside the wakes of the circular, SEF and N fin arrays.

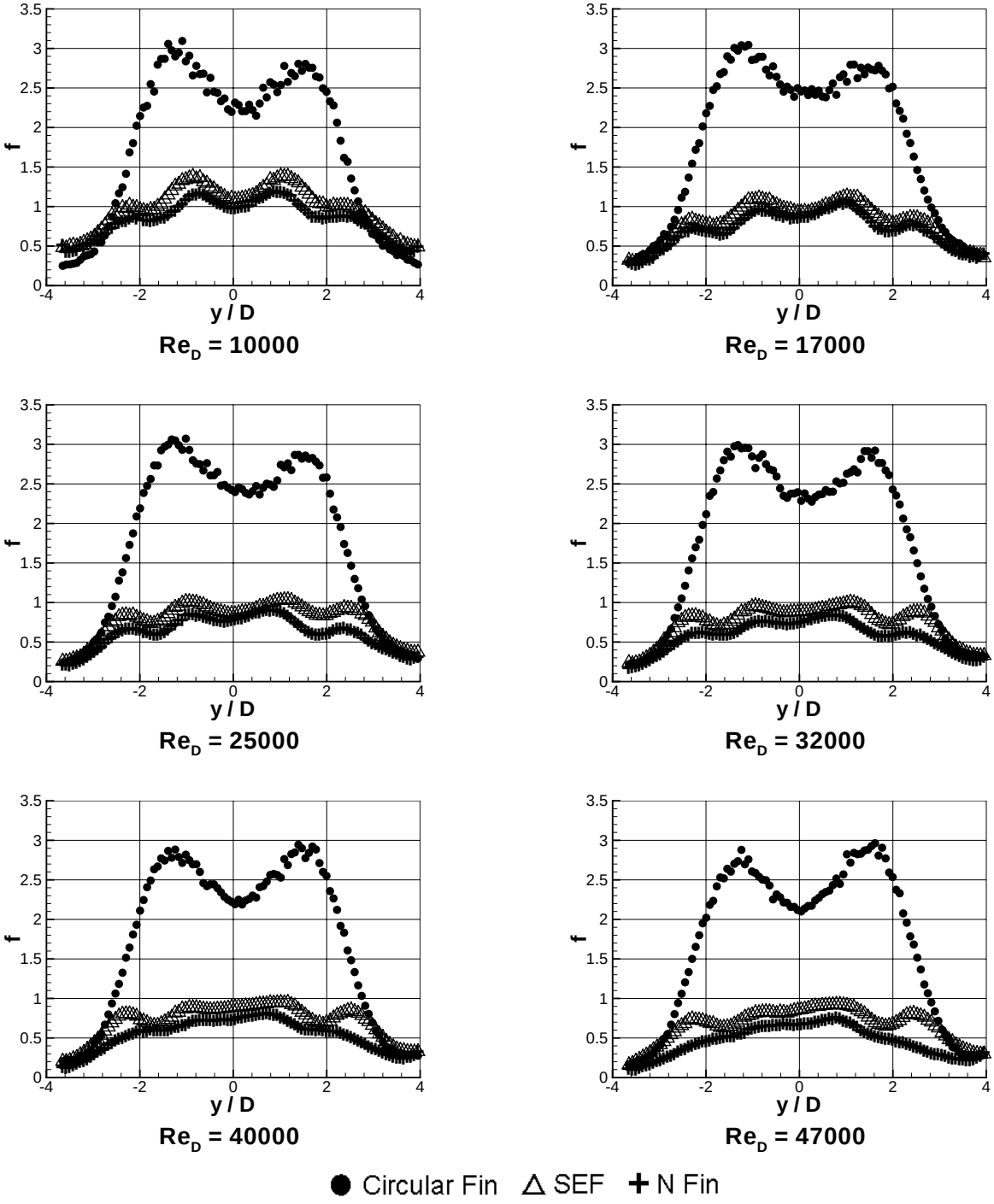

Figure 8. Friction Coefficient Distribution for Circular, SEF and N fin Arrays - 2D Downstream (X/D=2)

Significant reduction in the pressure loss levels is observed in the case of SEF and N fin arrays. The levels for the SEF and the N fin are close to each other, but N fin creates slightly less pressure loss inside the wake.

In case of the circular fin array, the wake region created by the two fins in the second row of the array are clearly visible in the form of two peaks in the friction coefficient distribution. Wakes of the fins in the first row are not visible individually but are all mixed up causing elevated pressure loss levels in the wake of the array. In case of the SEF and N fins, however, 4 separate peaks can be observed in the distributions. The middle two peaks are created due to the wake region of the two fins in the second row. The outer peaks are resulting from the pressure loss generated due to the wakes of the upper and lower fins in the first row in the array. This shows that the wakes of the first row fins do not mix with each other, but instead the localized losses created inside the individual wakes are carried downstream separately. The reason is that the SEF and the N fins create much smaller wake regions compared to the circular fins. The flow on the SEF and N fins does not separate until it gets very close to the downstream stagnation point due to the lack of sharp adverse pressure gradients on the bodies. However for a circular fin, very sharp pressure gradients exist on the body, which causes an early separation of the flow which in turn creates large wake regions when compared to the SEF and N fins. The pressure gradients on the N fins is even smoother than the SEF which causes the observed slightly less pressure loss levels due to a small reduction in the size of the wake.

Figure 9 shows the line averaged friction coefficient variation with inlet Reynolds number. As it can be seen from this figure, the circular fin array performs the worst in terms of pressure loss minimization. The N fin has the lowest pressure loss generation and the SEF has slightly higher levels in the Reynolds number range. If a quantitative comparison is made between the models by calculating the ratio of the average friction coefficient of the circular fins to the those of the SEF and N fins at the corresponding Reynolds numbers, it can be seen that the average loss levels for the circular fin are 78% and 106% higher than the levels of the SEF and N fins, respectively, for the lowest Reynolds number. For the highest Reynolds number, the circular fin has 158% and 270% more loss creation in average with respect to the SEF and N fins, respectively. This large difference

in the total pressure loss levels of these models makes the SEF and the N fin geometries very promising ones for efficient wall heat transfer enhancement applications. The equations for the best fit lines for the average friction loss are,

Circular Fin,

$$f = 2.302 Re_D^{-0.0157} Pr^{0.3} \tag{14}$$

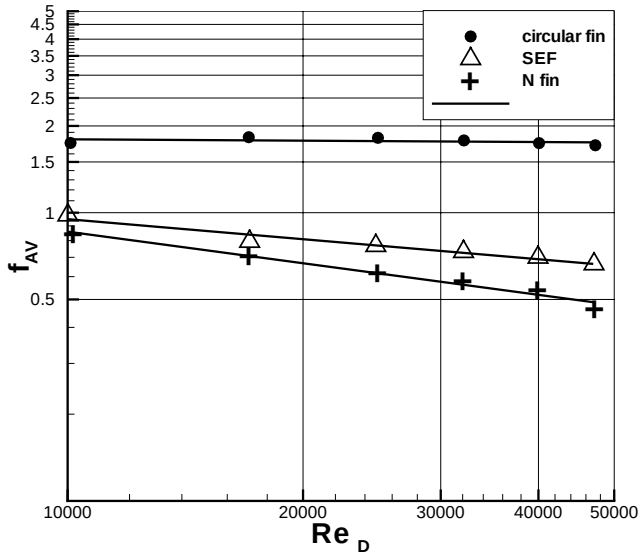

Figure 9. Average Friction Coefficient vs. Reynolds Number for Circular, SEF and N Fin Arrays

SEF,

$$f = 8.826 Re_D^{-0.231} Pr^{0.3} \tag{15}$$

N Fin,

$$f = 27.241 Re_D^{-0.364} Pr^{0.3} \tag{16}$$

Specific Friction Loss

A performance parameter is introduced at this stage as defined in Wang and Ji [4] to be able to compare different models more clearly, considering both the heat transfer enhancement and the pressure loss characteristics at different Reynolds numbers. This parameter is called the "specific friction loss" and is defined as,

$$\varepsilon_f = \frac{f_{av}}{Nu_{D_{av}}} \tag{17}$$

This parameter basically is an indication of the pressure loss levels for each model in order to achieve same amount of heat transfer capability on the wall inside the wake. Figure 10 shows the variation of this performance parameter for each model for different Reynolds numbers. It can be seen that the SEF and the N fin has much lower specific friction loss values than the circular fin. This can also be observed from Figure 11 in which the variation of the specific friction loss with the Reynolds number

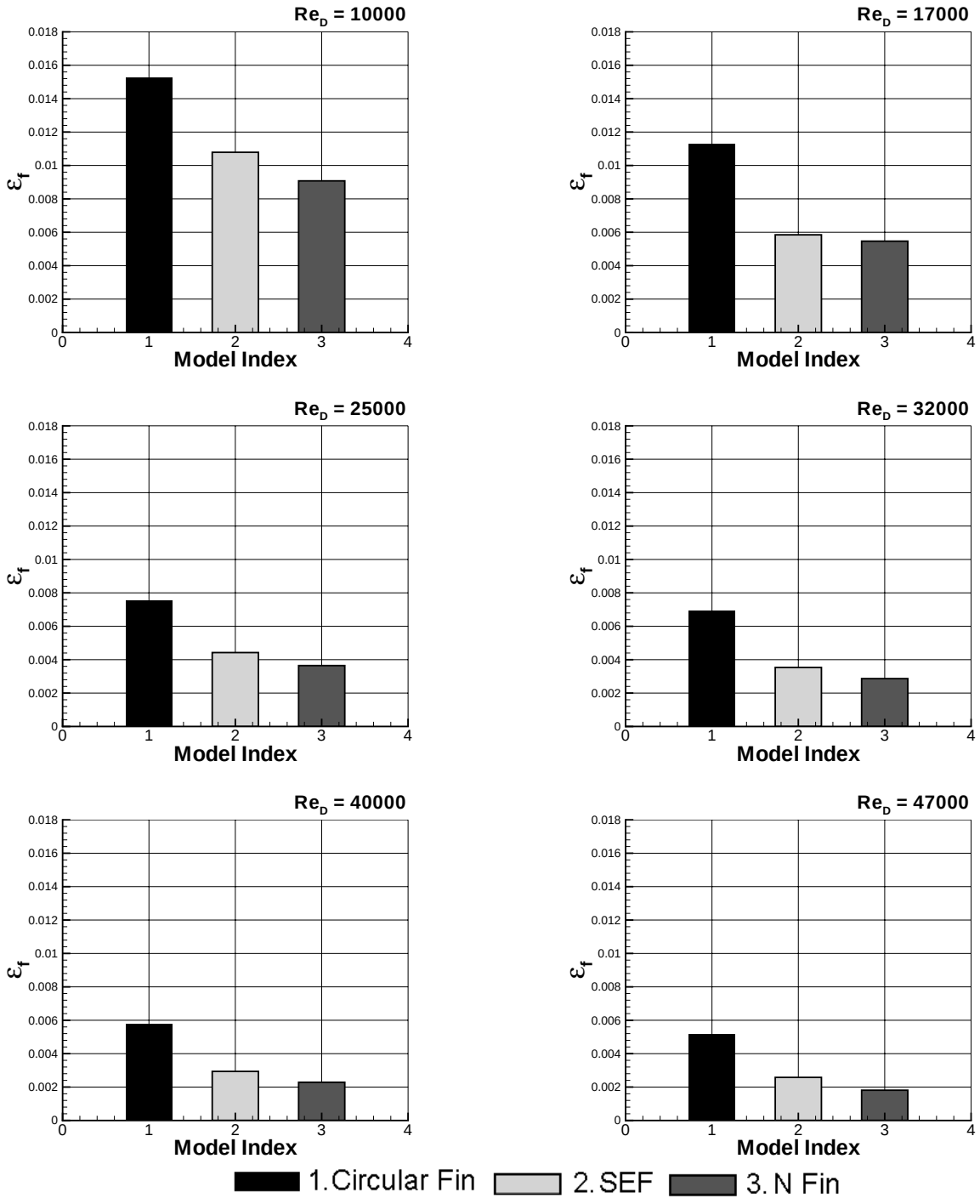

Figure 10. Specific Friction Loss at Different Reynolds Numbers

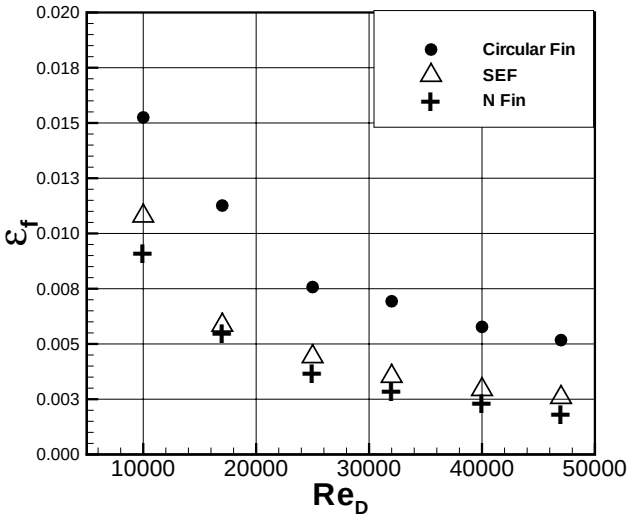

Figure 11. Specific Friction Loss Variation with Reynolds Number

is illustrated. Hence it can be concluded that the SEF and the N fin are much more effective fin shapes than the circular fin when both the heat transfer enhancement and pressure loss characteristics are considered.

CONCLUSIONS

Endwall heat transfer, total pressure loss measurements are conducted to determine the characteristics of the elliptical pin fins (SEF and the N fin) in array configurations and the results are compared to circular pin fin arrays. A staggered two row arrangement is used with fins having H/D=1.5 and S/D=X/D=2.

It is found that the heat transfer enhancement levels on the endwall inside the wake for the circular pin fin array is about 25% higher in average than the SEF and the N fin arrays. However, in terms of pressure loss, the SEF and the N fin arrays performed much better. Significant reductions in the aerodynamic penalty levels are observed. On average, the circular pin fin array caused 120% and 185% more pressure loss than the SEF and N fin arrays, respectively. As a result, even though the endwall heat transfer levels are about 25% are higher for circular pin fins, the tremendous reduction in total pressure loss levels makes the SEFs and N fins very attractive as alternatives to circular pin fins. These results become even more clear when the specific friction loss levels are compared. The alternative arrays of SEFs and N fins generate much less pressure loss for a unit gain in heat transfer enhancement.

Furthermore, the SEFs and the N fins will have a much better heat transfer enhancement characteristic on the fin itself due to increased wetted surface area such that there is a 35% increase for the SEFs and a 85% increase for the N fins. The SEF and N fin arrays will also be instrumental in improving the structural stiffness between the suction side and pressure side shells. The N fin arrays can also be used as flow divider elements at the trailing edge due to its elongated shape.

REFERENCES

[1] Steuber, G. D., Metzger, D. E., 1986, "Heat Transfer and Pressure Loss Performance for Families of Partial Length Pin Fin Arrays in High Aspect Ratio Rectangular Ducts," Proceedings of the 8^{th} International Heat Transfer Conference, Vol. 6, pp. 2915-2920.

[2] Arora, S. C., Abdel-Messeh, W., 1990, "Characteristics of Partial Length Circular Pin Fins As Heat Transfer Augmentors for Airfoil Internal Cooling Passages," Journal of Turbomachinery, **112**, pp. 559-565.

[3] Metzger, D. E., Fan, C. S., Haley, S. W., 1984, "Effects of Pin Shape and Array Orientation on Heat Transfer and Pressure Loss in Pin Fin Arrays," Journal of Engineering for Gas Turbines and Power, **106**, pp. 252-257.

[4] Wang, B. G., Ji, H. H., 1987, "An Experimental Investigation of Heat Transfer and Friction Loss in Taper Pin Fin Configurations of Air Cooled Turbine Blades," Proceedings of the ASME-JSME Thermal Engineering Joint Conference, Vol. 4, pp. 127-133.

[5] Grannis, V. B., Sparrow, E. M., 1991, "Numerical Simulation of Fluid Flow through an Array of Diamond Shaped Pin Fins," Numerical Heat Transfer, Part A, **19**, pp. 381-403.

[6] Minakami, K., Mochizuki, S., Murata, A., Yagi, Y., Iwasaki, H., 1992, "Visualization of Flow Mixing Mechanisms in Pin Fin Arrays," Proceedings of the International Symposium on Flow Visualization, pp. 504-508.

[7] Goldstein, R. J. and Jabbari, M. Y. and Chen, S. B., 1994 "Convective Mass Transfer and Pressure Loss Characteristics of Staggered Short Pin Fin Arrays," International Journal of Heat and Mass Transfer, **37**, pp. 149-160.

[8] Chyu. M. K., Hsing, Y. C., Natarajan, V., 1996, "Convective Heat Transfer of Cubic Pin Fin Arrays in a Narrow Channel," Presented at the International Gas Turbine and Aeroengine Congress and Exposition Birmingham, UK, 96-GT-201.

[9] Li, Q. and Chen, Z. and Flechtner, U. and Warnecke, H. J., 1998, "Heat Transfer and Pressure Drop Characteristics in Rectangular Channels with Elliptic Pin Fins," International Journal of Heat and Fluid Flow, **19**, pp. 245-250.

[10] Chen, Z., Li, Q., Meier, D., Warnecke, H. J., 1997, "Convective Heat Transfer and Pressure Loss in Rectangular Ducts with Drop-shaped Pin Fins," Heat and Mass Transfer, **33**, pp. 219-224.

[11] Uzol, O., Camci, C., 2001, "Elliptical Pin Fins as an Alternative to Circular Pin Fins for Gas Turbine Blade Cooling Applications Part 2: Wake Flow Field Measurements and Visu-

alizations using PIV," Presented at the 46th ASME International Gas Turbine, Aeroengine Congress and Exposition and Users Symposium, New Orleans, LA.

[12] Armstrong, J., Winstanley, D., 1988, "A Review of Staggered Array Pin Fin Heat Transfer for Turbine Cooling Applications," Journal of Turbomachinery, **110**, pp. 94-103.

[13] Abbott, I. H. and Von Doenhoff, A. E., 1959, *Theory of Wing Sections*, Dover Publications.

[14] Camci, C., Kim, K., Hippensteele, S. A., 1992, "A New Hue-Capturing Technique for the Quantitative Interpretation of Liquid Crystal Images Used in Convective Heat Transfer Studies," Journal of Turbomachinery, **114**, No. 4, pp. 765-775.

[15] Niblack, W., 1986, *An Introduction to Digital Image Processing*, Prentice/Hall International.

[16] Russ, J. C., 1995, *The Image Processing Handbook*, CRC Press.

[17] Wiedner, B. G., Camci, C., 1996, "Determination of Convective Heat Flux on Steady-State Heat Transfer Surfaces with Arbitrarily Specified Boundaries," Journal of Heat Transer, **118**, No. 4, pp. 1-8.

[18] Moffat, R. J., 1988, "Describing the Uncertainties in Experimental Results," Experimental Thermal and Fluid Science, **1**, pp. 3-17, 1988.

[19] Incropera, F. P., De Witt, D. P., 1990, *Introduction to Heat Transfer*, Second Edition, John Wiley and Sons Inc.

[20] Uzol, O., 2000, "Novel Concepts and Geometries As Alternatives to Conventional Circular Pin Fins for Gas Turbine Blade Cooling Applications," Ph.D. Thesis, Pennsylvania State University, University Park, PA.